Stability, folding dynamics, and long-range conformational transition of the synaptic t-SNARE complex

Xinming Zhang[a], Aleksander A. Rebane[a,b,c,d], Lu Ma[a], Feng Li[a,d], Junyi Jiao[a,b], Hong Qu[a], Frederic Pincet[a,d,e], James E. Rothman[a,d] & Yongli Zhang[a,[1]]

[a]Department of Cell Biology, Yale School of Medicine, [b]Integrated Graduate Program in Physical and Engineering Biology, [c]Department of Physics, Yale University, New Haven, CT 06511; [d]Nanobiology Institute, Yale University, West Haven, CT 06477; [e]Laboratoire de Physique Statistique, École Normale Superieure, L'université de recherche Paris Sciences et Lettres, CNRS UMR 8550, Sorbonne Universités, Université Pierre-et-Marie-Curie (UPMC) University of Paris 06, Université Paris Diderot, 75005 Paris, France.

Submitted to Proceedings of the National Academy of Sciences of the United States of America

Synaptic soluble N-ethylmaleimide-sensitive factor attachment protein receptors (SNAREs) couple their stepwise folding to fusion of synaptic vesicles with plasma membranes. In this process, three SNAREs assemble into a stable four-helix bundle. Arguably, the first and rate-limiting step of SNARE assembly is the formation of an activated binary t-SNARE complex on the plasma membrane, which then zippers with the v-SNARE on the vesicle to drive membrane fusion. However, the t-SNARE complex readily misfolds and its structure, stability, and dynamics are elusive. Using single-molecule force spectroscopy, we modeled synaptic t-SNARE complex as a parallel three-helix bundle with a small frayed C-terminus. The helical bundle sequentially folded in an N-terminal domain (NTD) and a C-terminal domain (CTD) separated by a central ionic layer, with total unfolding energy of ~17 k_BT. Peptide binding to the CTD activated the t-SNARE complex to initiate NTD zippering with the v-SNARE, a mechanism likely shared by Munc18-1. The NTD zippering then dramatically stabilized the CTD, facilitating further SNARE zippering. The subtle bidirectional t-SNARE conformational switch was mediated by the ionic layer. Thus, the t-SNARE complex acts as a switch to enable fast and controlled SNARE zippering required for synaptic vesicle fusion and neurotransmission.

T-SNARE complex | SNARE four-helix bundle | SNARE assembly | membrane fusion | optical tweezers

Synaptic SNAREs mediate fast and calcium-triggered fusion of synaptic vesicles to pre-synaptic plasma membranes required for neurotransmission (1). They consist of VAMP2 (also called synaptobrevin 2) anchored on vesicles (v-SNARE) and syntaxin and SNAP-25 located on target plasma membranes (t-SNAREs) (2). These SNAREs contain characteristic SNARE motifs of ~60 amino acids (3) (Fig. 1A). Syntaxin and SNAP-25 can form a 1:1 t-SNARE complex (4-6). During membrane fusion, the t- and v-SNAREs join to form an extraordinarily stable four-helix bundle (3, 7-10). In the core of the bundle are 15 layers of hydrophobic amino acids and a central ionic layer containing three glutamines and one arginine. Whereas the zippering energy and kinetics between t- and v-SNAREs have recently been measured (8, 9), the structure, stability, and dynamics of the t-SNARE complex have not been well understood.

The structure and dynamics of the t-SNARE complex are crucial for SNARE assembly and membrane fusion. Formation of the t-SNARE complex is likely an obligate intermediate prior to SNARE zippering (6, 11-14). A pre-formed t-SNARE complex docks the vesicles to plasma membranes (15) and boosts the speed, strength, and accuracy of SNARE zippering (5, 9, 16). Furthermore, the t-SNARE complex is an important target for proteins that regulate SNARE zippering and membrane fusion, such as Munc18-1, synaptotagmins, and complexin (8, 17-19). Finally, the t-SNARE complex shows intriguing dynamics in reconstituted membrane fusion. Peptides corresponding to the VAMP2 N-terminal domain (called Vn peptides or Vn) or C-terminal domain (Vc) are often used to facilitate membrane fusion (6, 10, 20, 21). Tightly bound to the t-SNARE complex, they attenuate SNARE zippering (8, 22), yet surprisingly enhance the rate of membrane fusion (6, 10). The underlying molecular mechanisms are not fully understood, which calls for an improved understanding of the structure and dynamics of the t-SNARE complex.

Studying t-SNARE folding is challenging using ensemble-based experimental approaches, because the t-SNARE complex readily misfolds (6, 21, 23) and is highly dynamic (4). Syntaxin and SNAP-25 can efficiently form a stable parallel four-helix bundle containing two syntaxin molecules and one SNAP-25 molecule (the 2:1 complex), which inhibits SNARE zippering and membrane fusion (5, 6). In addition, it is reported that the t-SNARE complex folds into at least two alternative conformations in which either SNARE motif in SNAP-25 partially or completely dissociates from syntaxin (4). Interestingly, the yeast t-SNARE homologs Sso1 and Sec9 do not misfold. Fiebig et al. found that Sso1 in the t-SNARE complex is N-terminally structured but C-terminally disordered (24). Using optical tweezers, Gao et al. observed that synaptic t-SNARE complexes unfold cooperatively

Significance

Intracellular membrane fusion is mediated by coupled folding and assembly of three or four SNARE proteins into a four-helix bundle. A rate-limiting step is the formation of a partial complex containing three helixes called the t- or Qabc-SNARE complex. The t-SNARE complex then serves as a template to guide stepwise zippering of the fourth helix, a process that is further regulated by other proteins. The synaptic t-SNARE complex readily misfolds. Consequently, its conformation, stability, and dynamics have not been well understood. Using optical tweezers and theoretical modeling, we elucidated the folding intermediates and kinetics of the t-SNARE complex and discovered a long-range conformational switch of t-SNAREs during SNARE zippering, which are essential for regulated SNARE assembly during synaptic vesicle fusion.

Reserved for Publication Footnotes

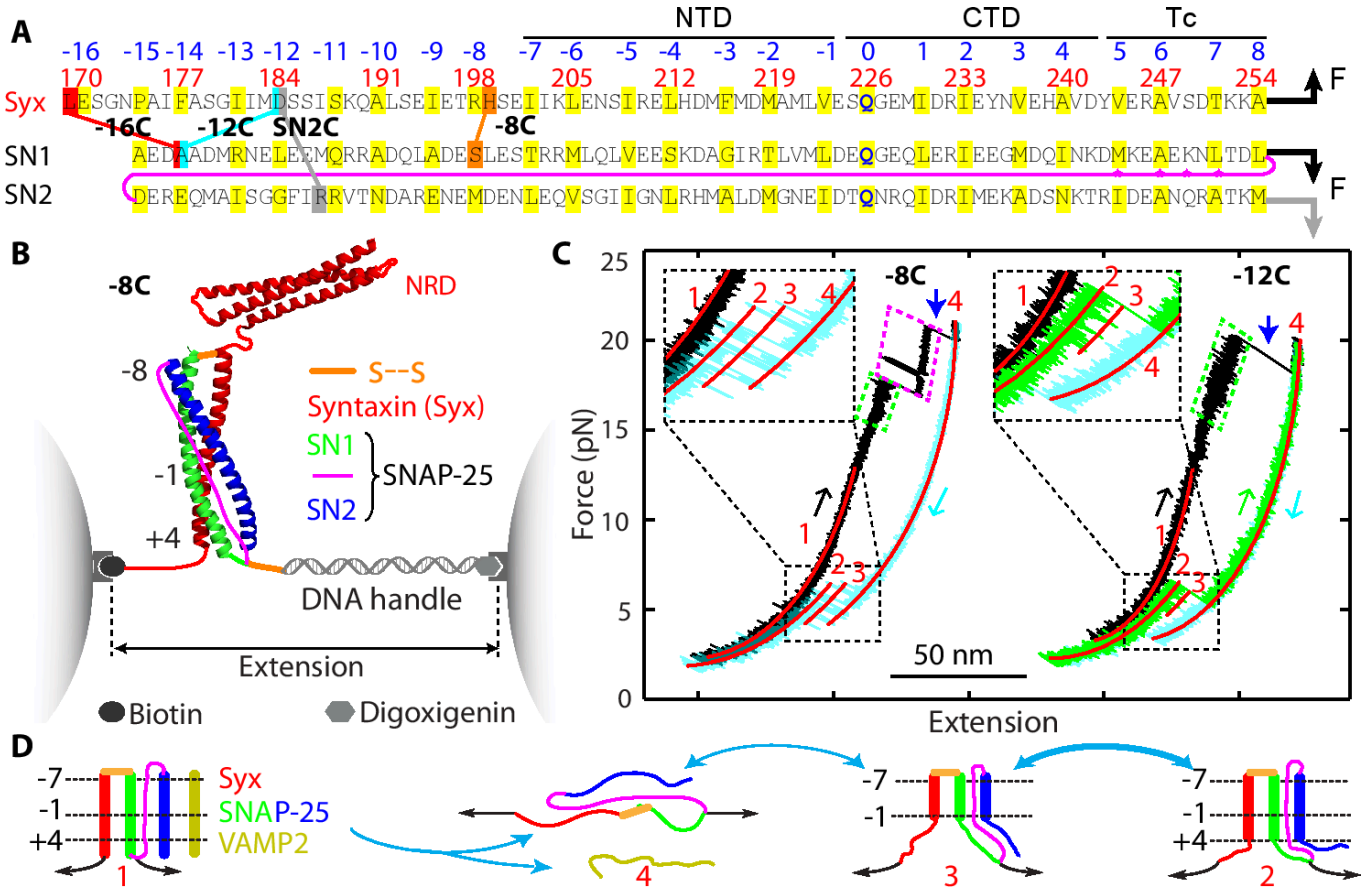

Fig. 1. T-SNARE sequences, experimental setup, and derived folding states. (A) Amino acids of the synaptic syntaxin 1A (Syx) and SNAP-25B containing SNARE motifs. SNAP-25B consists of two SNARE motifs (SN1 and SN2) connected by a disordered linker (magenta line), with four intrinsic cysteine (marked by stars) mutated to serine. Amino acids of the hydrophobic and ionic layers in the SNARE motifs (numbered from -7 to +8) and their N-terminal extensions (from -16 to -8) are highlighted in yellow. The syntaxin sequence is numbered in red. Four pairs of crosslinked amino acids are indicated by lines and labeled by their corresponding construct names and pulling sites (arrows). The t-SNARE complex contained three distinct folding domains: the N-terminal domain (NTD), the C-terminal domain (CTD), and the frayed t-SNARE C-terminus (Tc). (B) Experimental setup to pull a single t-SNARE complex (-8C) containing the N-terminal regulatory domain (NRD) of syntaxin. The structure of the folded t-SNARE complex shown here was modeled based on the crystal structure of the SNARE ternary complex (3) and our single-molecule measurements. (C) Force-extension curves (FECs) obtained by pulling (black and green) and relaxing (cyan) the two SNARE constructs -8C and -12C. The pulling or relaxing direction is indicated by arrows colored the same as the corresponding FECs. Blue arrows mark full disassembly of the ternary SNARE complex and accompanying dissociation of the VAMP2 molecule. Red lines are best fits of the corresponding FECs by the worm-like chain model. (D) Schematic of the SNARE transitions among four states, including the fully assembled ternary SNARE state 1, the folded t-SNARE state 2, the partially folded t-SNARE state 3, and the fully unfolded t-SNARE state 4.

at a high force when pulled from both ends of syntaxin, indicating a largely structured syntaxin in a stable t-SNARE complex (8, 9). However, the detailed conformation of the t-SNARE complex, especially SNAP-25, and its stability and dynamics are not clear.

In this work we measured the conformation, stability, and dynamics of a single synaptic t-SNARE complex using optical tweezers. Our single-molecule method prevented the t-SNARE complex from misfolding, allowing us to focus on the 1:1 complex. We found that the t-SNARE complex folded in two steps and had a frayed C-terminus (Tc). Binding of Vn stabilized the CTD, while binding of Vc stabilized NTD, structured Tc, and promoted initial ternary SNARE zippering, potentially accounting for the positive effect of both peptides on membrane fusion.

Results

T-SNARE constructs and experimental setup. To measure the conformation and stability of the cytoplasmic t-SNARE complex, we first pulled a single t-SNARE complex at the C-termini of syntaxin and the first SNARE motif in SNAP-25, or "SN1" (Fig. 1A,B). Their N-termini were crosslinked by a disulfide bond formed between two cysteine residues. We chose the N-terminal crosslinking site such that it facilitated refolding of the t-SNARE complex, but minimally altered its structure. We tested three crosslinking sites by substituting the corresponding amino acids with cysteine and designated the SNARE constructs as -8C, -12C, and -16C (Fig. 1A). To prevent t-SNARE misfolding and ensure correct crosslinking, we first formed the ternary SNARE complex and then removed the VAMP2 molecule by unfolding the ternary complex. The complex was attached on one end to a streptavidin-coated polystyrene bead through a biotinylated Avi-tag and on the other end to an anti-digoxigenin antibody-coated polystyrene bead through a 2,260 bp DNA handle (9) (Fig. 1B). The beads were trapped in two optical traps formed by focused laser beams. By moving one optical trap relative to the other, we controlled the force applied on the SNARE complex and measured the end-to-end extension of the SNARE-DNA tether in response to the force. We recorded the force and extension at 10 kHz and used them to derive t-SNARE folding and stability.

Syntaxin and SN1 are largely structured and fold reversibly. We first pulled a single ternary SNARE construct -8C to a force of ~22 pN, leading to a representative force-extension curve (FEC) shown in Fig. 1C. Below ~15 pN, the extension increased

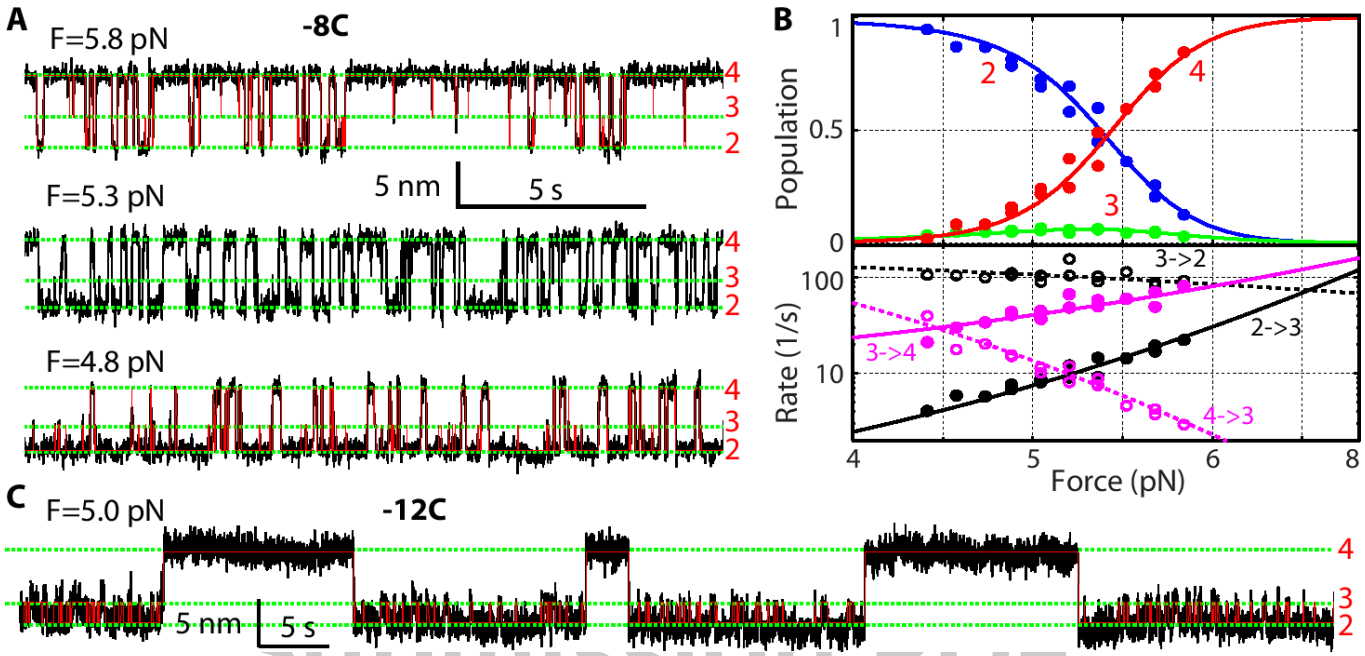

Fig. 2. Energetics and kinetics of three-state folding of the t-SNARE complex. (A) Extension-time trajectories that show reversible transitions of the t-SNARE complex (-8C) at the indicated constant mean force F. Red lines are idealized trajectories determined by hidden-Markov modeling (HMM) and green dashed lines mark the corresponding state positions. (B) Force-dependent probabilities of three t-SNARE folding states (top panel) and their associated transition rates (bottom panel). Experimental measurements (symbols) were fit by a theoretical model (solid lines, see "Materials and Methods"). (C) Extension-time trajectories of the t-SNARE complex (-12C). Idealized trajectories derived from HMM are shown as red lines.

Table 1. Domains and energies associated with t-SNARE folding. The C-terminal border of the CTD or NTD is shown by the number of the corresponding amino acid in syntaxin (Fig. 1A). The total dissociation energy in the last column was calculated as the sum of the CTD energy, the NTD energy, and the correction for the latter due to N-terminal crosslinking (Supporting Text and Table S1). Shown in the parenthesis is the standard deviation. The CTD of Syx Q226A is largely disordered (Fig. S6), and thus not accessed ("NA").

SNARE construct	C-terminal domain (CTD)		N-terminal domain (NTD)		Total dissociation energy (k_BT)
	Position (a.a)	Unfolding energy (k_BT)	Position (a.a.)	Unfolding energy (k_BT)	
-8C	243 (2)	7 (4)	222 (1)	5 (1)	17 (4)
Syx Q226A	NA	NA	233 (5)	6 (3)	11 (3)
Syx V244A	243 (5)	7 (4)	223 (3)	5 (2)	17 (4)
SN2C	243 (7)	6 (3)	222 (4)	6 (1)	18 (3)

monotonically with force, mainly due to stretching of the semi-flexible DNA handle. As a result, the FEC could be fit by a worm-like chain model (red curve) (25). Above 17 pN, first fast and then slow extension flickering (regions marked by green and magenta parallelograms, respectively) appeared successively as force increased, indicating reversible folding and unfolding transitions of a SNARE C-terminal region and middle region, respectively. At ~20 pN, an abrupt extension jump (indicated by a blue arrow) represented irreversible unfolding of the remaining N-terminal region. Pulling the molecule to above 20 pN did not cause any additional unfolding, which demonstrated that the SNARE complex had been fully unfolded (Fig. 1C, state 4). The above interpretations on SNARE transitions were confirmed by the similarities and differences in the FECs obtained by pulling the other two SNARE constructs -12C and -16C (Figs. 1C & S1).

Upon relaxation, the SNARE complex in all three constructs remained unfolded at a force above ~7 pN, but refolded below this force (Figs. 1C & S1). The folding process was reversible via a transient intermediate state (Fig. 1C,D, state 3). Interestingly, the fully refolded SNARE complex (in state 2) had an extension greater than the fully assembled ternary SNARE complex (in state 2), suggesting a partially folded t-SNARE complex. Pulling the t-SNAREs again revealed a FEC that overlapped the relaxation FEC (Fig. 1C, compare the green and cyan FECs for -12C). These observations indicates that the VAMP2 molecule dissociated from the t-SNAREs upon disassembly of the ternary complex. To confirm this interpretation, we added 10 μM VAMP2 into the solution after a single ternary SNARE complex had been disassembled and found that VAMP2 restored assembly of the ternary SNARE complex (Fig. S2). Thus, disassembly of the ternary SNARE complex led to dissociation of the VAMP2 molecule (Fig. 1D, from states 1 to 4) and generated an unfolded t-SNARE complex that partially refolded at a low force via an intermediate state 3. In addition, the intermediate state 3 ap-

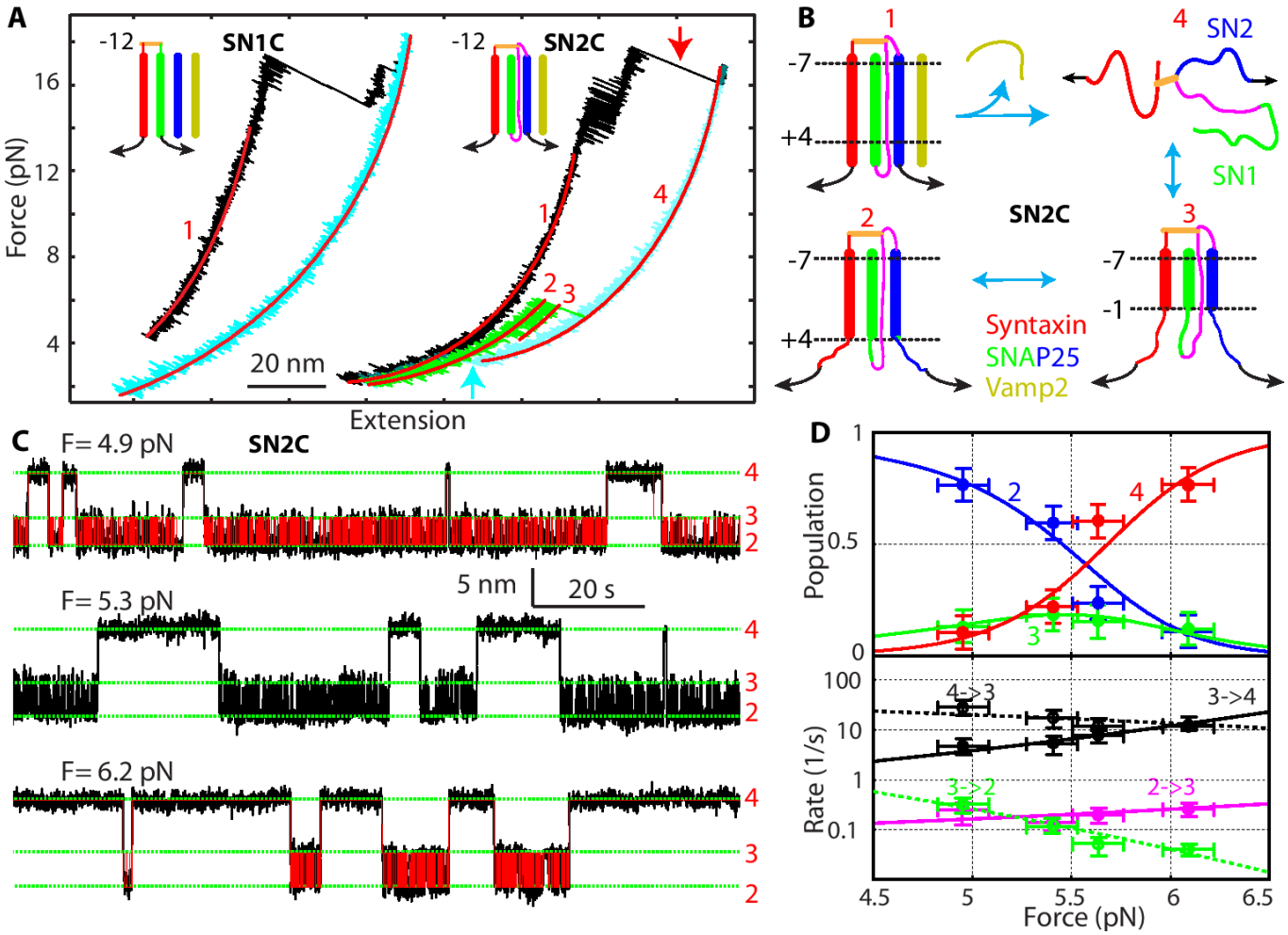

Fig. 3. . The three t-SNARE helices fold synchronously. (A) FECs obtained by first pulling (black) and then relaxing (cyan) the t-SNARE constructs SN1C and SN2C (insets). Further pulling SN2C led to the FEC shown in green. FEC regions were fit by the worm-like chain model (red lines), revealing different SNARE folding states (red numbers). (B) Schematic of the states and their transitions for SN2C. (C) Extension-time trajectories of SN2C at constant mean forces. The idealized extension transitions (red lines) were determined by three-state HMM and the average state extensions are marked by green dashed lines. (D) Force-dependent probabilities (top panel) and transition rates (bottom panel) associated with the different folding states of the t-SNARE complex SN2C. Results of model fitting are shown in solid lines. Error bars indicate standard deviations.

peared to be partially-zippered as is shown in Fig. 1D, because shifting the N-terminal crosslinking site away from the SNARE motifs (from -8C to -12C to -16C) changed the extension of the intermediate state relative to the extension of the unfolded t-SNARE state, but not of the folded t-SNARE state (Figs. 1C & S1). Finally, we found that the N-terminal regulatory domain (NRD) of syntaxin (Fig. 1B) did not significantly affect t-SNARE folding, as the t-SNARE complex without the NRD showed an identical FEC as the complex with the NRD (Fig. S3). This finding indicates that the NRD did not strongly interact with the SNARE motifs, consistent with our previous observation (8).

Structure, stability, and folding dynamics of the t-SNARE complex. To characterize t-SNARE folding at greater spatiotemporal resolution, we held the complex at constant mean forces in the range of 4-6 pN and detected its extension flickering caused by spontaneous t-SNARE transitions. Figure 2A shows three representative extension trajectories for construct -8C. We found that the t-SNARE complex folded and unfolded among states 2, 3, and 4 with distinct average extensions. We analyzed the extension trajectories using three-state hidden-Markov modeling (HMM) (8, 26, 27), which revealed idealized extension transitions (Fig. 2A) and best-fit model parameters, including state probabilities and transition rates (Fig. 2B). The intermediate state 3 had a population < 7% and a dwell time of 4-8 ms over the force range tested (Fig. S4). As force increased, the probabilities of the folded state 2 and the unfolded state 4 decreased and increased, respectively, and the probability of the intermediate state 3 first increased and then decreased (Fig. 2B, top). The observation suggests that the intermediate 3 was on-pathway for t-SNARE folding and unfolding. Indeed, the HMM shows that the rates of sequential transitions between states 4 and 3 and between states 3 and 2 were 20-1000 fold greater than the rate of direct transition between states 2 and 4. Accordingly, we ignored the non-sequential transitions in our subsequent analyses (Fig. 2B, bottom). To further confirm the t-SNARE transitions, we repeated the experiment using construct -12C (Fig. 2C). The larger loop introduced by crosslinking (Fig. 1A) dramatically slowed down the transition between states 3 and 4 (Figs. 2C & S4), as are observed in many other systems (28). Consequently, the intermediate state 3 was better resolved due to its greater lifetime (Fig. 2C). These findings confirm that the transition between states 3 and 4 was caused by the t-SNARE NTD (Fig. 1D). In contrast, the transition between states 3 and 2 was barely affected by the change in the crosslinking site, which corroborates the partially-zippered intermediate state 3.

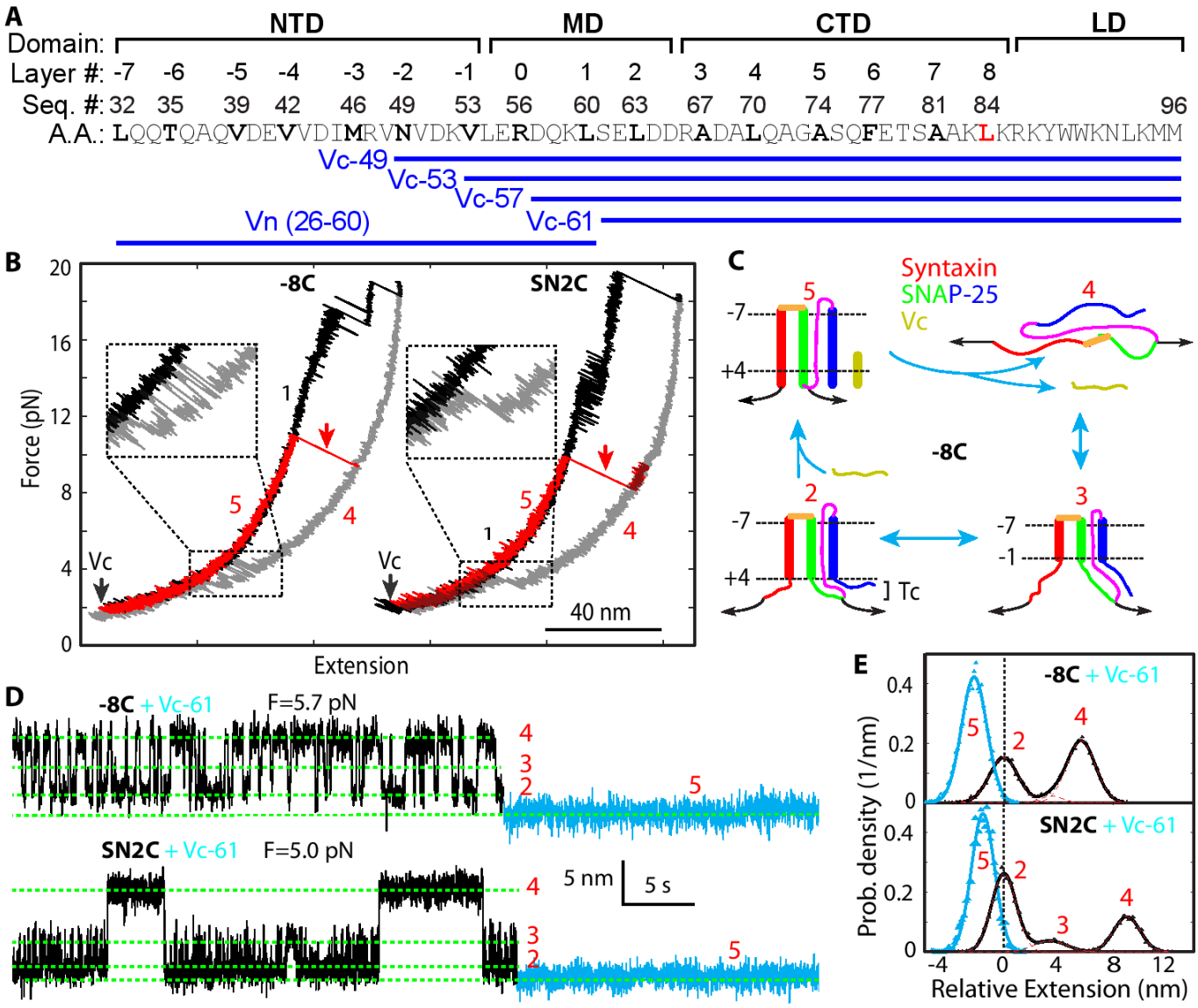

Fig. 4. Vc peptides induce Tc folding. (A) VAMP2, Vc, and Vn sequences and ternary SNARE zippering domains, including the middle domain (MD) and the linker domain (LD). (B) FECs of the t-SNARE complexes -8C and SN2C in the absence and presence of Vc. We first pulled to disassemble a ternary SNARE complex (black), then relaxed the t-SNARE complex (gray), added Vc (black arrows), and finally unfolded the Vc-bound t-SNARE complex (red FECs and arrows). (C) Schematic model of Vc-induced Tc folding in -8C. (D) Extension-time trajectories of the t-SNARE complexes -8C (top) and SN2C (bottom) at the indicated forces in the presence 0.5 μM Vc. The Vc-bound regions are highlighted in cyan. (E) Probability density distributions of the extensions in C (symbols with corresponding colors) and their best-fits by one Gaussian function or a sum of three Gaussian functions (lines). For the latter, individual Gaussian functions were plotted in red dashed lines.

To derive the conformations and folding energies of the partially zippered state and the folded state, we simultaneously fit the measured state populations, transition rates, forces, and extension changes using a theoretical model (26). The model treated the conformations and energies of different folding states at zero force as fitting parameters and accounted for all the experimental measurements under tension (Fig. 2B). We assumed that the three SNARE motifs synchronously zippered from the -7 layer towards the +8 layer, using the t-SNARE structure in the ternary complex as a template (3) (Materials and Methods). This assumption was tested by a series of experiments to be described below. Based on this inferred folding pathway, the positions of the partially-zippered state 3 and the folded state 2 were mainly determined by their extensions relative to the extension of the unfolded state 4. The model fitting showed that the folded t-SNARE complex was largely a three-helix bundle with frayed C-termini for both syntaxin and SN1. The boundary between the ordered and disordered regions lay approximately between the +4 and +5 layers (Table 1 and Fig. 1A). In the partially zippered state 3, the boundary was shifted to approximately -1 layer. Thus, the t-SNARE complex folded in two steps, first in the NTD (from -7 layer to -1 layer) and then in the CTD (from 0 layer to +4 layer). The model fitting also revealed unfolding energies of 5 k_BT for the NTD and of 7 k_BT for the CTD. A small barrier of 4 (±2) k_BT for CTD folding suggests a lifetime range of 7 – 400 μs for the intermediate state 3 at zero force. We derived a simple theory to relate the unimolecular NTD folding detected by us to bimolecular association between syntaxin and SNAP-25 (Supporting Text, Table S1, and Fig. S5). The theory yielded a binding energy of 17 k_BT or a dissociation constant of 41 nM and an apparent binding rate constant of 1.0×10^4 $M^{-1}s^{-1}$ between syntaxin and SNAP-25 (Tables 1 & S1). The binding

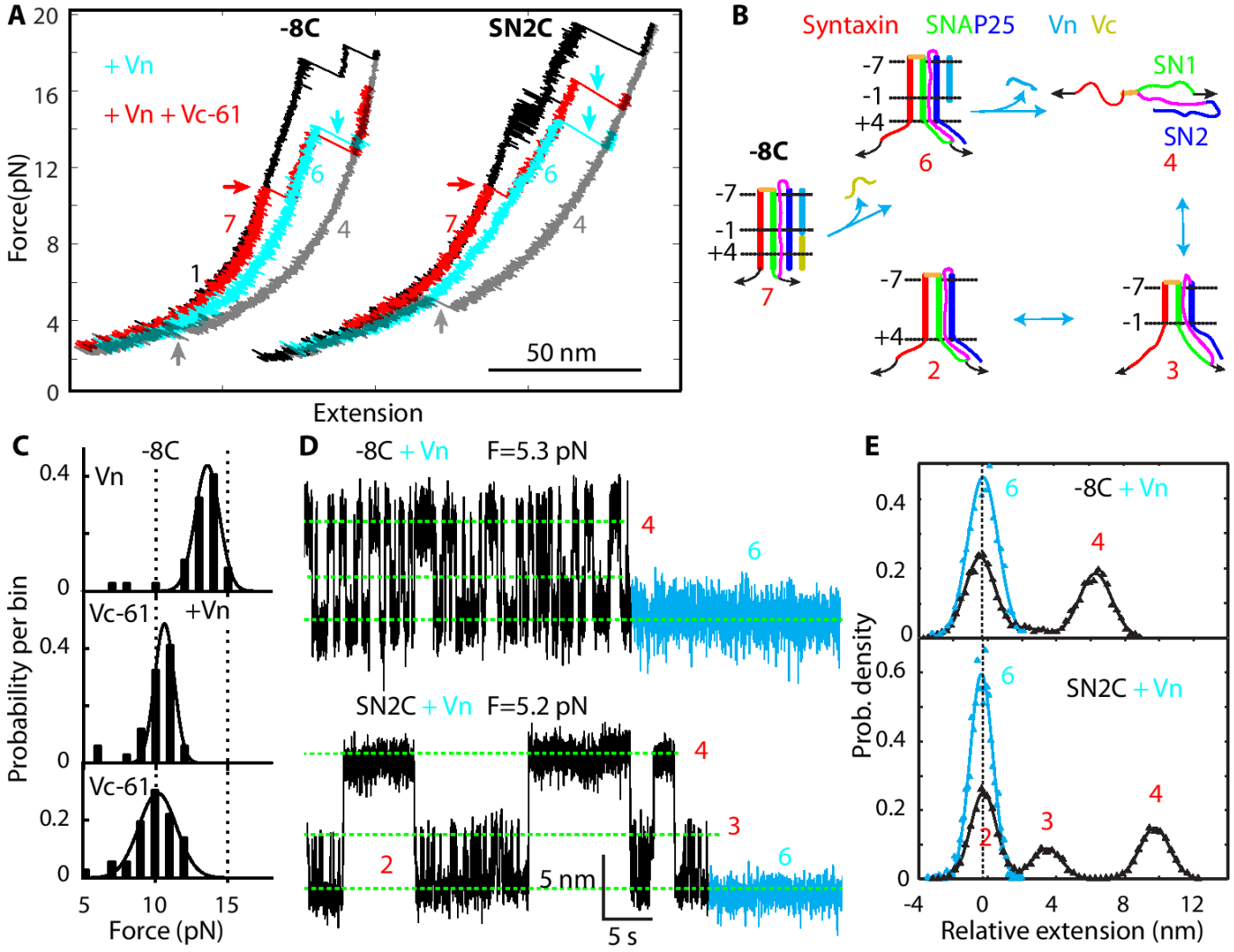

Fig. 5. Vn peptide stabilizes the CTD, but not Tc. (A) FECs obtained by pulling the t-SNARE complexes -8C and SN2C in the ternary SNARE complexes (black), in the presence of Vn (cyan) or both Vn and Vc (red). Events of Vn dissociation, Vc dissociation, and t-SNARE refolding are indicated by cyan, red, and gray arrows, respectively. (B) Schematic model that illustrates the states and transitions of the t-SNARE complex -8C in the presence of both Vn and Vc. (C) Histogram distribution of the unfolding force of the t-SNARE complex bound by Vn (top), both Vn and Vc (middle), or Vc only (bottom). In the presence of both Vn and Vc, the unfolding force is associated with the first unfolding event corresponding to Vc dissociation. (D) Extension-time trajectories of the t-SNARE complexes -8C and SN2C at constant mean forces F in 0.5 μM Vn. The Vn-bound states are highlighted in cyan. (E) Probability density distributions of the extension regions in black and cyan in C (symbols) and their best-fits by Gaussian functions (lines).

affinity and rate are consistent with previous measurements of 16 nM and 0.6×10^4 $M^{-1}s^{-1}$, respectively (5, 6). Our structural model for t-SNARE folding was confirmed by effects of single alanine substitutions in syntaxin, one at the ionic layer in the folded region ("Syx Q226A") and the other at the +5 layer in the disordered region ("Syx V244A"). As was predicted by the model, the former dramatically destabilized the t-SNARE complex and the latter barely changed t-SNARE folding (Table 1 and Fig. S6). This finding also show that the ionic layer plays an important role in stabilizing the t-SNARE complex. Finally, our model was further verified by pulling the t-SNARE complex from the N- and C-termini of syntaxin (Fig. S7) and the results below.

Three SNARE motifs fold synchronously. It was unclear what role SN2 played in the t-SNARE folding. To examine the impact of SN2, we split SNAP-25 in construct -12C into SN1 and SN2 and designated the quaternary SNARE construct as SN1C (Fig. 3A). Full disassembly of the complex led to dissociation of both VAMP2 and SN2, generating a syntaxin-SN1 conjugate. Relaxing the conjugate down to around zero force, we did not observe any folding event (Fig. 3A, cyan FEC). This finding demonstrated that SN2 was essential for t-SNARE folding and that syntaxin and SN1 could not form any stable structure. The t-SNARE structure derived by us contrasts with the previous t-SNARE structures in which SN2 can partially or completely dissociate (4, 29). Note that syntaxin and SN1 can associate into a four-helix bundle with two copies of each (16, 30), which cannot form under our experimental conditions. To further examine the SN2 conformation in the t-SNARE complex, we made a new t-SNARE construct designated as SN2C, in which the N-terminus of SN2 was crosslinked to syntaxin at the -12 layer (Figs. 3A & 1A). We now pulled the t-SNARE complex from the C-termini of SN2 and syntaxin and obtained representative FECs shown in Fig. 3A. After unfolding the ternary SNARE complex (red arrow), we relaxed the remaining t-SNAREs and saw their cooperative folding at ~3 pN (cyan arrow). The folded t-SNARE complex (in state 2) again had an extension greater than the corresponding ternary complex, confirming a frayed SN2 in Tc (Fig. 3B). Similar to -12C, further pulling the refolded SN2C caused a reversible transition between states 2 and 3 in the force range of 4-6 pN (Fig. 3A, green FEC). We then held the t-SNARE complex at constant

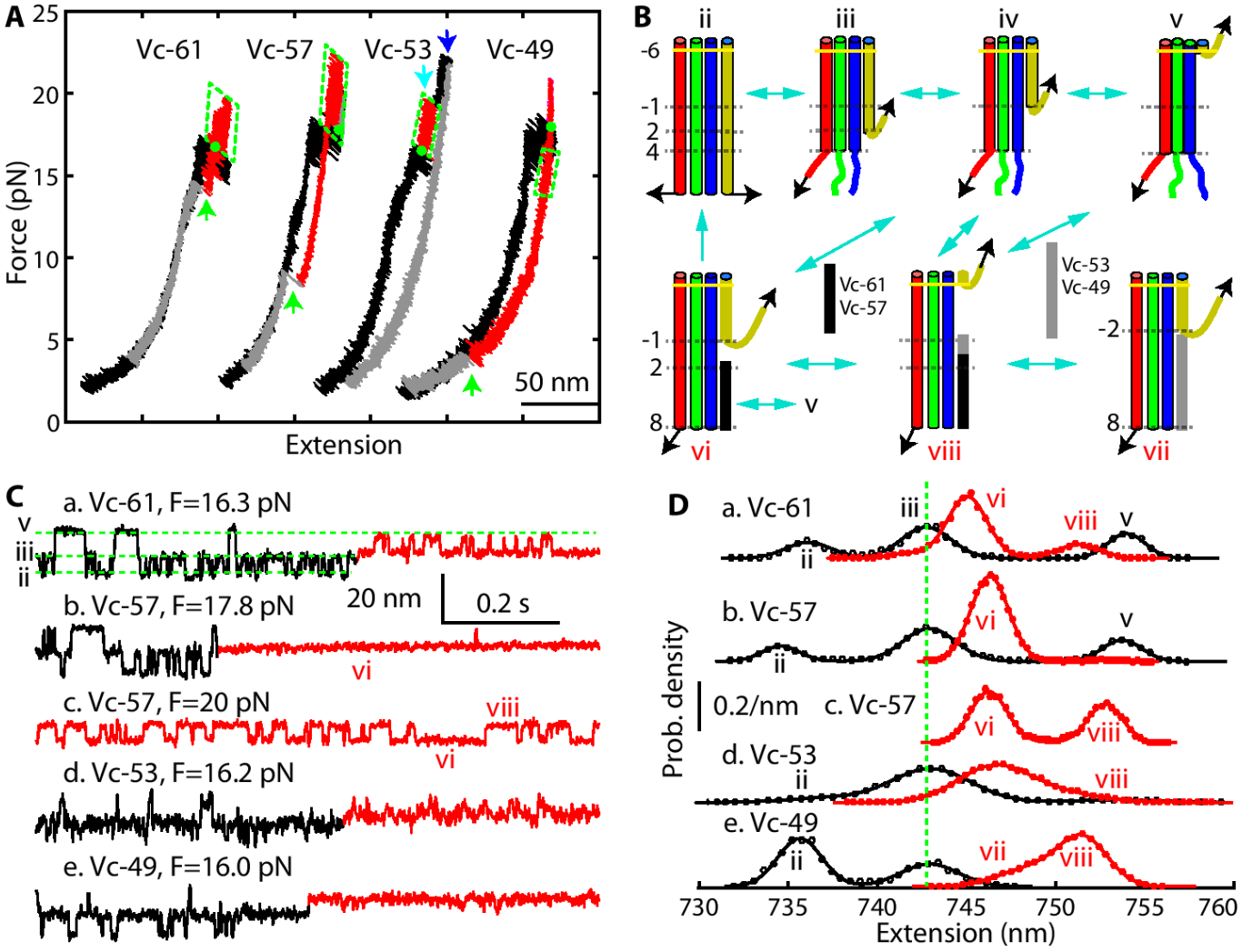

Fig. 6. Vc peptides enhance SNARE NTD association. (A) FECs obtained by pulling (black) and relaxing (grey) single ternary SNARE complexes in the presence of different Vc peptides. The Vc-bound SNARE states are shown in red as in C and D, with the NTD transitions marked by green dashed parallelograms. Vc peptides bound to SNARE complexes at green points and were displaced at points near green arrows. As a rare event, Vc-53 dissociated from the SNARE complex at a high force (marked by cyan arrow), followed by t-SNARE unfolding (blue arrow). The time-dependent force and extension corresponding to the FECs with Vc-57 are shown in Fig. S9A. (B) Diagram of different states and transitions involved in SNARE zippering and Vc binding, including the activated t-SNARE state viii. (C) Extension-time trajectories showing Vc binding at the indicated constant mean forces. Green dashed lines indicate the positions of different states shown in B. Extended views of two trajectories here are shown in Fig. S9B. (D) Probability density distributions of the extensions shown in C corresponding to the Vc-unbound states (black) and the Vc-bound states (red).

Table 2. Properties of the SNARE NTD folding in the absence (-) and presence of Vc peptides.

Vc peptide	Equilibrium force (pN)	Extension (nm)	Unfolding energy (k_BT)	Relative folding rate
-	17.2 (0.5)	6.7 (0.4)	24 (2)	1
Vc-61	18.1 (0.8)	6.7 (0.2)	25 (1)	6.0 (0.1)
Vc-57	20.2 (0.3)	6.7 (0.2)	29 (1)	5.8 (0.1)
Vc-53	18.0 (0.9)	5.2 (0.2)	19 (1)	4.1 (0.1)
Vc-49	15.0 (0.7)	4.3 (0.3)	12 (1)	1.4 (0.2)

mean forces and detected its force-dependent three-state transitions (Fig. 3C). Like -12C, the new construct exhibited a slow NTD transition and a fast CTD transition. Detailed analysis (Fig. 3D) showed that the conformations and unfolding energies of the t-SNARE complex derived from pulling SN2 are close to the corresponding measurements obtained from pulling SN1 (Table 1). These comparisons revealed that the three SNARE motifs in the t-SNARE complex zippered synchronously in two steps, first in NTD and then in CTD, and were all frayed in Tc (Fig. 1D). Compared to the half-zippered or highly dynamic t-SNARE structures previously reported (4, 10), the t-SNARE structure deduced by us is significantly more ordered and stable.

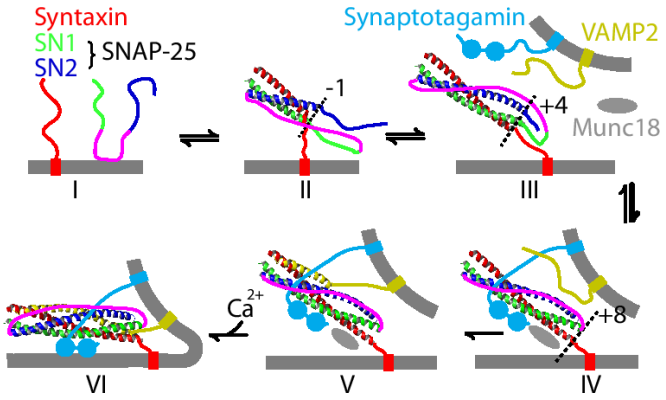

Fig. 7. . Model of t-SNARE folding and conformational changes in SNARE zippering and membrane fusion. The schematic states involved (not drawn to scale) are the monomeric t-SNAREs (I), the partially assembled t-SNARE complex (II), the folded t-SNARE complex (III), the activated t-SNARE complex (IV), the partially zippered trans-SNARE complex (V), and the zippered SNARE complex (VI).

Vc binding stabilizes the frayed Tc. To examine effects of Vc peptides on t-SNARE folding and ternary SNARE zippering, we tested four Vc peptides that start at different positions in the VAMP2 sequence but end at the same amino acid number 96 (Fig. 4A). These peptides are designated by "Vc-" followed by their starting amino acid numbers. We first pulled the t-SNARE constructs -8C and SN2C in the presence of 10 μM Vc-61 (10). After unfolding the ternary SNARE complexes (Fig. 4B, black FECs), we first refolded the t-SNARE complexes at a low force (gray FECs) and then added Vc-61 into the solution to allow Vc-61 to bind to the t-SNARE complexes (black arrows). In subsequent pulling, the Vc-bound t-SNARE complexes showed extensions identical to the ternary SNARE complex (Fig. 4B, compare red FECs to black FECs), indicating that Vc binding induced Tc folding as in the ternary complex (Fig. 4C, state 5). The Vc-bound t-SNARE complex completely unfolded at ~10 pN (Fig. 4B, red arrows), which suggests that Vc significantly enhanced the mechanical stability of the t-SNARE complex.

To further observe the Vc-induced disorder-to-helix transition in Tc, we held the t-SNARE complex at a constant mean force in the presence of 0.5 μM Vc-61. For both constructs -8C and SN2C, we first observed reversible three-state transitions characteristic of the free t-SNARE complex (Fig. 4D, black regions). Then, the transitions stopped at a low extension, consistent with the Vc-bound t-SNARE state (cyan regions). The t-SNARE complex remained in the Vc-bound state for more than 20 minutes, corroborating a strong association between Vc and the t-SNARE complex. The Vc-bound state 5 in both -8C and SN2C had an extension that was 2-4 nm lower than that of the folded t-SNARE complex in state 2, with an average of 2.6 (±0.4) nm (Fig. 4D-E). The extension change is consistent with folding of the whole Tc, which extends our previous observation on the Vc-induced folding in the frayed syntaxin C-terminus (8).

Vn binding stabilizes the CTD, but not Tc. Li *et al*. recently demonstrated that the t-SNARE complex pre-bound by Vn also greatly promotes SNARE-mediated membrane fusion (10). To pinpoint its underlying mechanism, we investigated the effect of Vn on t-SNARE folding (Fig. 4A). In the presence of 10 μM Vn, the t-SNARE complex initially showed the same extension as the folded t-SNARE state 2 at a low force (Fig. 5A, compare cyan and gray FECs), indicating that Vn bound to the t-SNARE complex, but did not induce Tc folding (Fig. 5B, state 6). However, unlike the free t-SNARE complex, the Vn-bound t-SNARE complex remained in the folded state to a high force typically around 13 pN. Then the complex abruptly and completely unfolded (Fig. 5A, cyan arrows, Fig. 5B, from states 6 to 4). The unfolding force of the Vn-bound t-SNARE complex approximately followed a Gaussian distribution (Fig. 5C, top). The average unfolding force 13.4 (±1.6) pN was significantly higher than the average equilibrium unfolding force of the t-SNARE complex alone, or ~5.4 pN (Fig. 2B). These observations indicate that Vn greatly stabilized the t-SNARE CTD. To confirm this finding, we examined Vn binding at a constant mean force. For both -8C and SN2C, Vn binding trapped the t-SNARE complex in a low extension state (Fig. 5D, cyan regions). A comparison of the extension probability density distributions of the Vn-bound and -unbound states showed that the Vn-bound t-SNARE state 6 had an extension identical to the folded t-SNARE state 2 (Fig. 5E). The finding confirms that Vn stabilized CTD, but not Tc (Fig. 5B). Moreover, lengthening the Vn peptide to the +3 layer led to the same conclusion (Fig. S8), indicating a common role of Vn peptides in specifically stabilizing the CTD. Finally, the Vn-induced CTD stabilization is further supported by our experiments in the presence of both Vn and Vc peptides (Fig. 5A-C). Interestingly, Tc unfolding was enough to dissociate Vc (Fig. 5B, from states 7 to 6). As a result, the distribution of the force to dissociate Vc did not significantly depend on Vn (Fig. 5C, compare middle and bottom panels). Therefore, a structured Tc is required for SNARE CTD zippering. In conclusion, our results suggest that Vn binding significantly stabilized the CTD, but did not induce CTD folding, in contrast to a recent derivation (10).

Effect of t-SNARE conformational switch on ternary SNARE zippering. We have recently shown that the t- and v-SNAREs zipper stepwise in three distinct domains, the NTD, the middle domain (MD), and the CTD (8) (Fig. 4A), in a manner similar to stepwise t-SNARE folding reported here. In particular, the NTDs of both the ternary SNARE complex and the t-SNARE complex correspond to the same hydrophobic layers from -7 to -1. Our above Vn-binding experiment suggests that as VAMP2 zippers to MD, the t-SNARE CTD is stabilized and forms a rigid template for the v-SNARE to zipper, thereby promoting the speed and energy of SNARE zippering. This observation at least partly explains why Vn peptides enhance membrane fusion (10). However, it remains unclear how Vc peptides stimulate membrane fusion (6, 20), given their role in attenuating v-SNARE zippering (8). To further pinpoint the effect of Vc peptides on SNARE zippering, we repeated our SNARE zippering assay (8) in the presence of four Vc peptides with different lengths (Figs. 4A & 6A). Here, a ternary SNARE complex was crosslinked between syntaxin and VAMP2 near their -6 layers and pulled from their C-termini in the presence of 50 μM Vc peptides (Fig. 6B). The FECs showed the folding states and pathways of the SNARE complex alone as previously reported (Figs. 6A & S9A, black and grey curves, and Fig. 6B, states ii-v) (8). However, the FECs also contained new features from the Vc-bound SNARE complexes (Figs. 6A & S9A, red curves). Vc binding occurred in the force range of the overlapping CTD, MD, and NTD transitions (Fig. 6A, green dots), which suggests that Vc bound to the t-SNARE complex after VAMP2 was partially or completely unzipped or destabilized by force (Fig. 6B). The bound Vc was generally displaced at a low force, as was manifested by an extension drop during relaxation (Fig. 6A, green arrows, and Fig. 6B, from state vi or vii to state ii). The Vc displacing force was stochastic and dependent on the length of the Vc peptide, with a smaller average displacing force for a longer Vc peptide (Fig. 6A).

Vc binding dramatically changed the energetics of ternary SNARE zippering. Because Vc binding blocked CTD and MD folding, the CTD and MD transitions were inhibited and only the two-state NTD transition remained (Figs. 6C & S9B). Vc binding changed the NTD stability in a length-dependent manner, as is indicated by changes in the equilibrium between the folded and the unfolded NTD states and their equilibrium forces (Table 2).

For example, at a constant mean force of 17.8 pN (Fig. 6C, black region in trace b), the SNARE complex frequently unzipped. However, upon Vc-57 binding the complex primarily resided in the folded NTD state (red region in trace b). The equilibrium change was also demonstrated by the change in the extension probability density distribution (Fig. 6D, compare black and red curves). As a result, frequent NTD transition was only seen at a higher force near its equilibrium force of ~20 pN (Fig. 6C-D). In addition, Vc-57 binding did not alter the average extension change accompanying the NTD transition (Fig. 6D and Table 2), ruling out any large structural change in NTD induced by Vc-57. These observations indicated that Vc-57 binding significantly stabilized NTD by inducing a subtle long-range conformational change, likely helix packing, in the t-SNARE complex. In contrast, Vc-53 and Vc-49 destabilized NTD transition (Table 2), because both peptides partially blocked NTD folding (Fig. 4A) and decreased the extension changes of NTD transitions (Fig. 6D and Table 2). Based on extensive measurements of force-dependent NTD transitions, we derived NTD unfolding energies in the presence of four Vc peptides (Table 2). Whereas Vc-61 only slightly stabilized the NTD, Vc-57 increased the NTD unfolding energy by 5 (±2) k_BT, significantly stabilizing the NTD. This comparison suggests that the ionic layer mediated the Vc-induced t-SNARE conformational switch that stabilized the NTD. In contrast, Vc-53 and Vc-49 destabilized the NTD progressively, as both peptides impeded NTD zippering.

Vc peptides also enhanced the rate of NTD folding in a length-dependent manner (Figs. 6C, S9B, and Table 2). The NTD of the native SNARE complex slowly assembles but readily disassembles upon vesicle undocking (8, 9), limiting the overall rate of SNARE assembly and membrane fusion. Munc18-1 and other regulatory proteins enhance NTD assembly to initiate SNARE zippering (17, 31, 32). Vc-57 significantly increased the rate and stability of NTD assembly, suggesting that this peptide efficiently activated the t-SNARE complex to initiate SNARE zippering. Other Vc peptides are predicted to promote SNARE zippering in a descending efficiency order of Vc-61, Vc-53, and Vc-49, consistent with their order of potency to activate membrane fusion (20). Vc-49 has widely been used to facilitate SNARE-mediated fusion (6, 20). Our results suggest that Vc-49 significantly destabilized NTD and only slightly enhanced the rate of NTD zippering. However, Vc-49 binds to the t-SNARE complex with the highest affinity among the four Vc peptides and may additionally promote SNARE zippering and membrane fusion by stabilizing the t-SNARE complex in the 1:1 complex (6). Alternatively, Vc peptides inhibit SNARE mis-assembly, such as formation of anti-parallel SNARE bundles, thereby indirectly promoting functional SNARE assembly and membrane fusion (19). Note that the two mechanisms of Vc-enhanced SNARE assembly are not necessarily exclusive: the increased rate or energy of NTD zippering decreases the yield of SNARE mis-assembly due to kinetic or thermodynamic partitioning of the two processes. We expect that the N-terminal crosslinking in our SNARE constructs did not change the relative stability and rate of NTD assembly measured by us (Table 2 and Supplementary Text). Our results demonstrate that Vc peptides not only enhanced the rate of NTD zippering (33), but also could stabilize the NTD in a length-dependent manner. Interestingly, Munc18-1 stabilized Tc and NTD zippering in a manner similar to Vc-57 (8), suggesting a common mechanism to directly or indirectly promote initial SNARE zippering and membrane fusion by regulating the t-SNARE conformation.

Discussion

Using optical tweezers, we measured the folding intermediates, energies, and kinetics of the synaptic t-SNARE complex and probed its long-range conformational change during SNARE zippering using Vn and Vc peptides. We derived a structural model for the t-SNARE complex in which the three SNARE motifs formed a three-helix bundle from -7 to +4 layers and were disordered from +5 to +8 layers. Our structural derivation assumed a particular t-SNARE folding pathway ("Materials and Methods") and a homogeneous worm-like chain model for the polypeptide. We verified the derived structures by measurements on the t-SNARE complexes that were not crosslinked, crosslinked at four N-terminal sites, pulled from three different sites, mutated in syntaxin, split in SNAP-25, or bound by Vn and Vc. In contrast to other t-SNARE models (4, 10), the t-SNARE structure derived by us contains a fully ordered binding site (from -4 to +3 layers) for synaptotagmin (18) and a largely ordered binding site for complexin (19, 34). T-SNARE folding was robust under our experimental conditions. Thus, our results revealed a significantly more structured and stable t-SNARE complex than previous derivations and corroborated the bidirectional t-SNARE conformational change crucial for fast and regulated SNARE zippering (4, 8, 10, 24, 33). However, we did not test t-SNARE misfolding into the 2:1 complex, which is expected to be the primary t-SNARE misfolding pathway. In addition, t-SNARE stability and dynamics may be altered by membranes (4, 35), which were absent in our experiments.

We propose a model to describe t-SNARE folding during membrane fusion (Fig. 7). First, the t-SNARE NTD slowly associates, forming the partially assembled t-SNARE complex (from states I to II). Subsequently, this complex spontaneously and reversibly folds into the full t-SNARE complex (state III). Synaptotagmin and Munc18-1 then bind to the t-SNARE complex, docking the vesicle to the plasma membrane (state IV) (14, 15, 18). Munc18-1 stabilizes the t-SNARE complex, which is required for efficient docking (15). Furthermore, Munc18-1 induces Tc folding and the NTD conformational change, activating the t-SNARE complex to initiate SNARE zippering (8, 32, 33). Note that Munc18-1 also binds to SNAREs in other modes that play crucial roles in SNARE assembly (8, 14, 31). Binding of v-SNARE NTD forms a half-zippered trans-SNARE complex, a process that is assisted by synaptotagmins, complexin, and other proteins (1, 19, 31) (state V). The v-SNARE binding also stabilizes the t-SNARE CTD in the force-bearing trans-SNARE complex, which in turn stabilizes associations of regulatory proteins to the trans-SNARE complex. Finally, calcium triggers further zippering of v-SNARE along the stabilized t-SNARE template, leading to fast assembly of the SNARE four-helix bundle and subsequent membrane fusion (state VI).

Materials and Methods

SNARE proteins. The syntaxin construct comprised the cytoplasmic domain of rat syntaxin 1A (residues 1-265, with mutation C145S), a spacer sequence (GGSGNGGSGS), and a C-terminal Avi-tag (GLNDIFEAQKIEWHE). The genes corresponding to the syntaxin protein and mouse VAMP2 (residues 28-94) were cloned into the pET-SUMO vector (Thermo Fisher), while the SNAP-25B gene was inserted into the pET-28a vector. All proteins were expressed in BL21 (DE3) cells and purified using Ni-NTA beads. The syntaxin protein was biotinylated in vitro using biotin ligase enzyme (BirA) as previously described (8, 9). The N-terminal His-tag and SUMO protein were cleaved from the purified syntaxin and VAMP2 proteins. Syntaxin, SNAP-25 and VAMP2 were mixed in a molar ratio 1:1: 2 in HEPES buffer containing 10 mM imidazole and 2 mM tris(2-carboxyethyl)phosphine (TCEP). Ternary SNARE complexes were formed by incubating the mixture at 4 °C overnight and then purified using the N-terminal His-tag on SNAP-25.

High-resolution dual-trap optical tweezers. The optical tweezers were home-built as described (8). Briefly, a 1064 nm laser beam was expanded, collimated, and split into two orthogonally polarized beams. The beams were focused by a water-immersion objective with a numerical aperture of 1.2 (Olympus, PA) to form two optical traps. Displacements of the trapped beads were detected by back-focal plane interferometry. Optical tweezers were remotely operated through a computer interface written in LabVIEW (National Instruments, TX).

Single-molecule protein folding experiment. The purified SNARE complexes were crosslinked with the DNA handle as described before (9). An aliquot of the crosslinked protein-DNA conjugate was incubated with 1 µL anti-digoxigenin coated polystyrene beads 2.17 µm in diameter (Spherotech,

IL), diluted to 1 mL phosphate-buffered saline (PBS), and injected into the top channel of a microfluidic chamber. Streptavidin coated polystyrene beads of 1.86 μm were injected into the bottom channel. Both top and bottom channels were connected to a central channel by capillary tubes, where both kinds of beads were trapped. A single SNARE complex was tethered between two beads by bringing them close. Data were recorded at 20 kHz, mean-filtered to 10 kHz, and stored on a hard disc. The single-molecule experiment was conducted in PBS at 23 (±1) °C. An oxygen scavenging system was added to prevent potential protein photo-damage by optical traps.

Data analysis. Our methods were described in detail elsewhere (9, 26, 27). Briefly, the extension trajectories were analyzed by two- or three-state hidden-Markov modeling (HMM), which yielded the probability, extension, force, lifetime, and transition rates for each state (27). To relate the experimental measurements to the conformations and energy (or the energy landscape) of the t-SNARE complex at zero force, we constructed a structural model for t-SNARE folding (26). In this model, three SNARE motifs were assumed to synchronously zippered layer by layer from the -7 layer towards the +8 layer, which established a t-SNARE folding pathway as a function of the reaction coordinate, the contour length of the unfolded polypeptide stretched by optical tweezers. We chose the contour lengths and folding energies of the partially zippered and the folded t-SNARE complexes as fitting parameters, which allowed us to calculate the total extension of the SNARE-DNA tether and the total energy of the tether and beads in optical traps. The extension and energy of the unfolded polypeptide, as well as the DNA handle, were calculated using the Marko-Siggia formula (25). The extension of the folded portion was derived from the t-SNARE structure in the ternary SNARE complex. From the calculated total energies for all states, we further evaluated the probability of each state based on the Boltzmann distribution and transition rates based on the Kramers' equation. Finally, we fit the calculated state extensions, forces, probabilities, and transition rates to the corresponding experimental measurements using nonlinear least-squares fitting, which revealed the conformations and energies of different t-SNARE folding states as best-fit parameters.

Acknowledgements

We thank Axel Brunger and Erdem Karatekin for discussion and Tong Shu for help. This work was supported by the NIH grants GM093341 to Y. Z., GM071458 to J. R., and T32GM007223, and by the Raymond and Beverly Sackler Institute at Yale. X. Z., L. M., J. R., and Y. Z. designed the experiments, X. Z, L. M, F. L., J. J., and H. Q. performed the experiments, all authors analyzed the data, and Y. Z., X. Z. wrote the paper. The authors declare no interest of conflict.

1. Sudhof TC, Rothman JE (2009) Membrane fusion: grappling with SNARE and SM proteins. *Science* 323:474-477.
2. Sollner T, Whiteheart SW, Brunner M, Erdjument-Bromage H, Geromanos S, Tempst P, Rothman JE (1993) SNAP receptors implicated in vesicle targeting and fusion. *Nature* 362:318-324.
3. Sutton RB, Fasshauer D, Jahn R, Brunger AT (1998) Crystal structure of a SNARE complex involved in synaptic exocytosis at 2.4 angstrom resolution. *Nature* 395:347-353.
4. Weninger K, Bowen ME, Choi UB, Chu S, Brunger AT (2008) Accessory proteins stabilize the acceptor complex for synaptobrevin, the 1 : 1 syntaxin/SNAP-25 complex. *Structure* 16:308-320.
5. Fasshauer D, Margittai M (2004) A transient N-terminal interaction of SNAP-25 and syntaxin nucleates SNARE assembly. *J Biol Chem* 279:7613-7621.
6. Pobbati AV, Stein A, Fasshauer D (2006) N- to C-terminal SNARE complex assembly promotes rapid membrane fusion. *Science* 313:673-676.
7. Walter AM, Wiederhold K, Bruns D, Fasshauer D, Sorensen JB (2010) Synaptobrevin N-terminally bound to syntaxin-SNAP-25 defines the primed vesicle state in regulated exocytosis. *J Cell Biol* 188:401-413.
8. Ma L, Rebane AA, Yang G, Xi Z, Kang Y, Gao Y, Zhang YL (2016) Munc18-1-regulated stage-wise SNARE assembly underlying synaptic exocytosis. *eLIFE* 4:e09580.
9. Gao Y, Zorman S, Gundersen G, Xi ZQ, Ma L, Sirinakis G, Rothman JE, Zhang YL (2012) Single reconstituted neuronal SNARE complexes zipper in three distinct stages. *Science* 337:1340-1343.
10. Li F, Kummel D, Coleman J, Reinisch KM, Rothman JE, Pincet F (2014) A half-zippered snare complex represents a functional intermediate in membrane fusion. *J Am Chem Soc* 136:3456-3464.
11. Weber T, Zemelman BV, McNew JA, Westermann B, Gmachl M, Parlati F, Sollner TH, Rothman JE (1998) SNAREpins: Minimal machinery for membrane fusion. *Cell* 92:759-772.
12. Pertsinidis A, Mukherjee K, Sharma M, Pang ZPP, Park SR, Zhang YX, Brunger AT, Sudhof TC, Chu S (2013) Ultrahigh-resolution imaging reveals formation of neuronal SNARE/Munc18 complexes in situ. *Proc Natl Acad Sci USA* 110:E2812-E2820.
13. Knowles MK, Barg S, Wan L, Midorikawa M, Chen X, Almers W (2010) Single secretory granules of live cells recruit syntaxin-1 and synaptosomal associated protein 25 (SNAP-25) in large copy numbers. *Proc Natl Acad Sci USA* 107:20810-20815.
14. Dawidowski D, Cafiso DS (2016) Munc18-1 and the Syntaxin-1 N terminus regulate open-closed states in a t-SNARE complex. *Structure* 24:392-400.
15. de Wit H, Walter AM, Milosevic I, Gulyas-Kovacs A, Riedel D, Sorensen JB, Verhage M (2009) Synaptotagmin-1 docks secretory vesicles to syntaxin-1/SNAP-25 acceptor complexes. *Cell* 138:935-946.
16. Fasshauer D, Eliason WK, Brunger AT, Jahn R (1998) Identification of a minimal core of the synaptic SNARE complex sufficient for reversible assembly and disassembly. *Biochemistry-Us* 37:10354-10362.
17. Shen JS, Tareste DC, Paumet F, Rothman JE, Melia TJ (2007) Selective activation of cognate SNAREpins by Sec1/Munc18 proteins. *Cell* 128:183-195.
18. Zhou QJ, *et al.* (2015) Architecture of the synaptotagmin-SNARE machinery for neuronal exocytosis. *Nature* 525:62-67.
19. Choi UB, Zhao ML, Zhang YX, Lai Y, Brunger AT (2016) Complexin induces a conformational change at the membrane-proximal C-terminal end of the SNARE complex. *Elife* 5:e16886.
20. Melia TJ, Weber T, McNew JA, Fisher LE, Johnston RJ, Parlati F, Mahal LK, Sollner TH, Rothman JE (2002) Regulation of membrane fusion by the membrane-proximal coil of the t-SNARE during zippering of SNAREpins. *J Cell Biol* 158:929-940.
21. Kreutzberger AJB, Liang BY, Kiessling V, Tamm LK (2016) Assembly and comparison of plasma membrane SNARE acceptor complexes. *Biophys J* 110:2147-2150.
22. Hernandez JM, Stein A, Behrmann E, Riedel D, Cypionka A, Farsi Z, Walla PJ, Raunser S, Jahn R (2012) Membrane fusion intermediates via directional and full assembly of the SNARE complex. *Science* 336:1581-1584.
23. Liu W, Stout RF, Jr., Parpura V (2012) Ternary SNARE complexes in parallel versus anti-parallel orientation: examination of their disassembly using single-molecule force spectroscopy. *Cell Calcium* 52:241-249.
24. Fiebig KM, Rice LM, Pollock E, Brunger AT (1999) Folding intermediates of SNARE complex assembly. *Nat Struct Biol* 6:117-123.
25. Marko JF, Siggia ED (1995) Stretching DNA. *Macromolecules* 28:8759-8770.
26. Rebane AA, Ma L, Zhang YL (2016) Structure-based derivation of protein folding intermediates and energies from optical tweezers. *Biophys J* 110:441-454.
27. Zhang YL, Jiao J, Rebane AA (2016) Hidden Markov modeling with detailed balance and its application to single protein folding *Biophys J* 111:In press.
28. Woodside MT, Behnke-Parks WM, Larizadeh K, Travers K, Herschlag D, Block SM (2006) Nanomechanical measurements of the sequence-dependent folding landscapes of single nucleic acid hairpins. *Proc Natl Acad Sci USA* 103:6190-6195.
29. An SJ, Almers W (2004) Tracking SNARE complex formation in live endocrine cells. *Science* 306:1042-1046.
30. Misura KMS, Gonzalez LC, May AP, Scheller RH, Weis WI (2001) Crystal structure and biophysical properties of a complex between the N-terminal SNARE region of SNAP25 and syntaxin 1a. *J Biol Chem* 276:41301-41309.
31. Baker RW, Jeffrey PD, Zick M, Phillips BP, Wickner WT, Hughson FM (2015) A direct role for the Sec1/Munc18-family protein Vps33 as a template for SNARE assembly. *Science* 349:1111-1114.
32. Munch AS, *et al.* (2016) Extension of Helix 12 in Munc18-1 induces vesicle priming. *J Neurosci* 36:6881-6891.
33. Li F, Tiwari N, Rothman JE, Pincet F (2016) Kinetic barriers to SNAREpin assembly in the regulation of membrane docking/priming and fusion. *Proc Natl Acad Sci U S A* 113:10536-10541.
34. Kummel D, Krishnakumar SS, Radoff DT, Li F, Giraudo CG, Pincet F, Rothman JE, Reinisch KM (2011) Complexin cross-links prefusion SNAREs into a zigzag array. *Nat Struct Mol Biol* 18:927-933.
35. Su ZL, Ishitsuka Y, Ha T, Shin YK (2008) The SNARE complex from yeast is partially unstructured on the membrane. *Structure* 16:1138-1146.
36. Moran LB, Schneider JP, Kentsis A, Reddy GA, Sosnick TR (1999) Transition state heterogeneity in GCN4 coiled coil folding studied by using multisite mutations and crosslinking. *Proc Natl Acad Sci USA* 96:10699-10704.
37. Rognoni L, Stigler J, Pelz B, Ylanne J, Rief M (2012) Dynamic force sensing of filamin revealed in single-molecule experiments. *Proc Natl Acad Sci USA* 109:19679-19684.
38. Gao Y, Sirinakis G, Zhang YL (2011) Highly anisotropic stability and folding kinetics of a single coiled coil protein under mechanical tension. *J Am Chem Soc* 133:12749–12757.
39. Plischke M, Bergersen B (2006) *Equilibrium statistical physics* (World Scientific Publishing Co., Singapore) 3rd Ed.
40. Kiema T, Lad Y, Jiang PJ, Oxley CL, Baldassarre M, Wegener KL, Campbell ID, Ylanne J, Calderwood DA (2006) The molecular basis of filamin binding to integrins and competition with talin. *Mol Cell* 21:337-347.